Detection of Raindrop with Various Shapes on a Windshield

Junki Ishizuka and Kazunori Onoguchi
Hirosaki University, 3 Bunkyo-cho, Hirosaki, Aomori, Japan

Keywords: ITS, Edge Ratio, Texture Analysis.

Abstract: This paper presents the method to detect raindrops with various shapes on a windshield from an in-vehicle single camera. Raindrops on a windshield causes various bad influence for video-based automobile applications, such as pedestrian detection, lane detection and so on. Therefore, it's important to understand the state of the raindrop on a windshield for a driving safety support system or an automatic driving vehicle. Although conventional methods are considered on isolated spherical raindrops, our method can be applied to raindrops with various shapes, e.g. a band-like shape. In the daytime, our method detects raindrop candidates by examining the difference of the blur between the surrounding areas. We uses the ratio of the edge strength extracted from two kinds of smoothed images as the degree of the blur. At night, bright areas whose intensity does not change so much are detected as raindrops.

1 INTRODUCTION

Recently, a vehicle equipped with a video camera is increasing to support safe driving. Since this camera is usually installed behind the front windshield of a vehicle, raindrops on a windshield disturbs the visibility and causes false detection in various video-based automobile applications. For example, it's difficult to detect the preceding vehicle in Fig.1 because this vehicle blurs by adherent raindrops on a windshield. For this reason, it's important to detect raindrops on a windshield for a driving safety support system or an autonomous vehicle.

A person can recognize raindrops on a windshield easily in spite of a background. However, it's difficult problem to understand the state of the raindrop from an image taken through a windshield since a raindrop mixes with a texture in a background. Moreover, a raindrop on a windshield blurs because a camera usually focuses on a background. This makes raindrop detection more difficult.

Garg and Nayer (Garg and Nayar, 2007) proposed the method to detect rain streaks in video sequences using intensity property of rain streaks for the first time. Since then, various methods containing snow detection (Barnum et al., 2010) have been proposed. However, these methods cannot be applied to a raindrop on a windshield because they model falling raindrops. Although the device which detects a raindrop on a windshield by an IR sensor has been produced to activate a windshield wiper automatically, it sometimes makes a wiper malfunction since the detection region covered by an IR sensor is too narrow to cover driver's visibility.

Several methods using a video camera have been proposed to detect a raindrop on a windshield since a video camera has wide detection region. Kurihata et al. (Kurihata et al., 2005) used a subspace method to extract raindrops. This method created a raindrop template, so called eigendrops, by PCA from images and showed good results only in the area with few textures, such as in the sky. They improved the performance in the high textured area by matching detection result between several frames (Kurihata et al., 2007). Halimeh et al. (Halimeh and Roser, 2009) proposed the method based on a geometric-photometric model that described the refractive property of a raindrop on a windshield. Although this model assumed that the shape of a raindrop on a windshield was a section of a sphere, Sugimoto et al. (Sugimoto et al., 2012) extended this assumption to a spheroid section. Liao et al. (Liao et al., 2013) detected raindrops on a windshield based on three characteristics that a raindrop exists in the video frames for a period of time, its shape is close to an ellipse and it is bright. Nashashibi et al. (Nashashibi et al., 2010) detected unfocus raindrops using the similar characteristics. Eigen et al. (Eigen et al., 2013) removed small dirt or raindrops from a corrupt image by predicting a clean output by convolutional neural network. You et al. (You et al., 2013) detected a small round area, in which the

Ishizuka, J. and Onoguchi, K.
Detection of Raindrop with Various Shapes on aWindshield.
DOI: 10.5220/0005796004750483
In *Proceedings of the 5th International Conference on Pattern Recognition Applications and Methods (ICPRAM 2016)*, pages 475-483
ISBN: 978-989-758-173-1

Figure 1: Raindrops on a front windshield of a vehicle.

Figure 2: Raindrops on textured background and non-textured background.

brightness change was small and the motion was slow, as a raindrop. Conventional methods described above are considered on isolated spherical raindrops. However, when it rains hard, raindrops are connected on a windshield and show various shapes even if a windshield wiper is activated. As shown in Fig.1, band-like shapes may appear on a windshield because of wiping. In this paper, we proposes the method to detect raindrops with various shapes on a windshield in the daytime and at night. This paper is organized as follows. Section 2.1 describes the detail for detecting raindrops on a windshield in the daytime. Section 2.2 describes the detail for detecting raindrops on a windshield at night. Section 3 discusses experimental results performed to several road scenes. Conclusions are presented in Sect. 4.

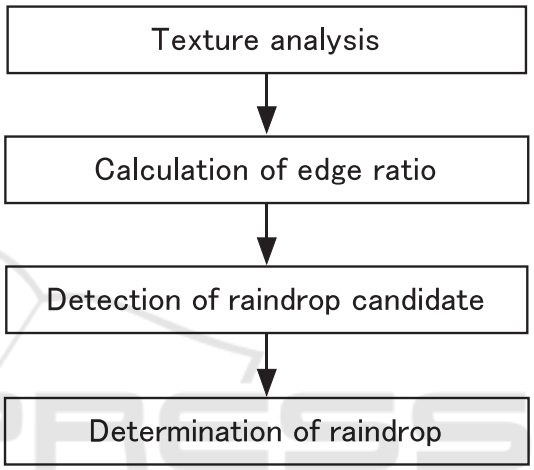

Figure 3: Outline of the proposed method.

2 RAINDROP DETECTION METHOD

Different algorithms are used in the daytime and at night since the appearance of a raindrop is quite different. Our method judges the day or night by the intensity level of the whole image or an in-vehicle illuminance sensor.

2.1 Raindrop Detection in the Daytime

Our method assumes that a raindrop in the daytime has the bellow characteristics.

1. When the texture of the background is strong, a raindrop on a windshield blurs more than its neighbourhood, as shown in the upper red rectangle of Fig.2.
2. When the texture of the background is weak, a raindrop has stronger texture than its neighbourhood, as shown in the lower red rectangle of Fig.2, because an intensity change occurs in the boundary of a raindrop.

Our method detects a raindrop by examining the degree of the blur between a raindrop area and its surrounding area. Figure 3 shows the outline of raindrop detection method in the daytime. At first, an input image is divided into strong textured areas and weak textured areas. Next, the ratio of edge strength extracted from two kinds of smoothed images is calculated as the degree of the blur. Raindrop candidates are detected from the change of edge ratio. Finally, misdetection areas are removed from raindrop candidates using the characteristic that raindrops on a windshield don't move so much. The details of each step are described below.

2.1.1 Texture Analysis

An input image is divided into grid blocks $B(u,v)$ $(1 \leq u \leq N, 1 \leq v \leq M)$. Texture analysis based on the edge strength is conducted in each block. In experiments, the image size is 640×360 pixels and the size of each block $B(u,v)$ is 10×10 pixels. Sobel operator is applied for edge detection and the total of the edge strength $E(u,v)$ is calculated in each block $B(u,v)$. $B(u,v)$ is classified into a textured block when $E(u,v)$

(a) Input image.

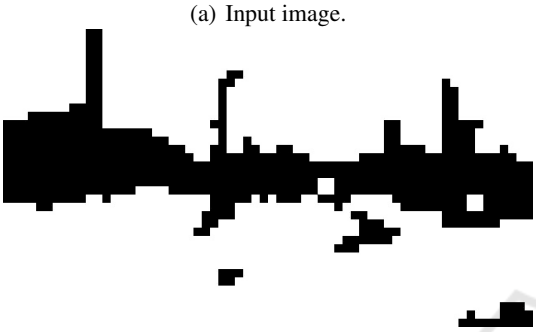

(b) Segmentation result.

Figure 4: Textured block and non-textured block.

is larger than T_E. Otherwise, $B(u,v)$ is classified into a non-textured block when $E(u,v)$ is smaller than T_E. The threshold T_E is determined so that a road surface may be included in a non-textured block. Figure 4(b) shows the example classifying each block into a textured block and non-textured block. A black block shows a textured block and a white block shows a non-textured block.

2.1.2 Detection of Raindrop Candidate

Our method detects raindrop candidates using the characteristic that the degree of the blur is different between a raindrop region and its neighbourhood. In order to measure the degree of the blur without depending on the texture of the background, the ratio of edge strength extracted from two kinds of smoothed images is calculated. An input image $I(i,j)$ $(1 \leq i \leq W, 1 \leq j \leq H)$ is smoothed by the Gaussian filter. Let $I_{s1}(i,j)$ denote an image smoothed by the Gaussian filter whose variance is σ_1 and let $I_{s2}(i,j)$ denote an image smoothed by the Gaussian filter whose variance is σ_2. σ_2 is larger than σ_1. Edge strength images $I_{e1}(i,j)$ and $I_{e2}(i,j)$ are created by applying the Sobel operator to $I_{s1}(i,j)$ and $I_{s2}(i,j)$. Edge strength greatly changes by smoothing in the area where the texture is clear. On the other hand, the change of the edge strength is small in the area where the texture blurs. The degree of the blur $D_b(i,j)$ at the pixel (i,j) is defined by

$$D_b(i,j) = \frac{I_{e1}(i,j)}{I_{e2}(i,j)} \tag{1}$$

$D_b(i,j)$ is small at the pixel where the degree of the blur is severe, but it's large at the pixel where the degree of the blur is light. Therefore, $D_b(i,j)$ of a raindrop is smaller than that of neighbouring regions when the background has clear strong texture and $D_b(i,j)$ of a raindrop is larger than that of neighbouring regions when the background is homogeneous. The raster scanning is conducted in $D_b(i,j)$ $(1 \leq i \leq W, 1 \leq i \leq H)$ and raindrop candidates are detected using two following conditions.

1. The pixel (i,j) is included in the non-textured block.

   The pixel (i,j) is chosen as a raindrop candidate when there are one or more neighbourhood pixels (k,l) $(i-1 \leq k \leq i+1, j-1 \leq l \leq j+1)$ satisfying $D_b(i,j) - D_b(k,l) > T_n$.

2. The pixel (i,j) is included in the textured block.

   The pixel (i,j) is chosen as a raindrop candidate when there are one or more neighbourhood pixels (k,l) $(i-1 \leq k \leq i+1, j-1 \leq l \leq j+1)$ satisfying $D_b(k,l) - D_b(i,j) > T_t$.

In experiments, T_n and T_t are set to 0.78 and 2.1. In Fig.5(b), pixels satisfying these conditions are indicated by white points. The neighbourhood pixel (k,l) satisfying $\mid D_b(i,j) - D_b(k,l) \mid < T_c$ is added to raindrop candidates until a new raindrop candidate is not detected. In experiments, T_c is set to 0.1. Figure 5(c) shows the final result of raindrop candidates.

2.1.3 Determination of Raindrop

Raindrop candidates contain some false areas, such as edge areas in surrounding structures. Our method removes these areas by integrating the detection results of several frames since the motion of a background is large but that of a raindrop on a windshield is small in an image. At first, the binary image $R_t(i,j)$ $(1 \leq i \leq W, 1 \leq j \leq H)$ in which raindrop candidates are set to 1 is created in each frame t. Next, an integration image $SR(i,j)$ is created by adding $R_{t-n+1}(i,j), R_{t-n+2}(i,j), \cdots, R_t(i,j)$. $SR(i,j)$ is binarized by the predetermined threshold T_r. In experiments, n and T_r are set to 3 and 2 respectively.

When a vehicle moves along a road, some areas on the straight line toward the vanishing point, such as on the guardrail, the railing of the bridge or the boundary of the wall, may be detected wrongly because the similar texture appears continuously. In order to remove these areas, the direction of the optical flow is examined in raindrop candidates. The motion detected on the lane marker and so on converges at

the vanishing point. On the other hand, the motion detected in a raindrop is unstable. For this reason, our method detects the optical flow in the raindrop candidate and calculates the variance of the flow direction in the block whose center is the pixel of interest for 15 frames. In experiments, the block size is 11×11. Figure 6 (a)-(c) show the example of the optical flow detected in the raindrop candidate shown in Fig.5(c). Figure 6 (d) shows the histogram of the flow direction in the raindrop (blue circle) and Fig. 6(e) shows the histogram of the flow direction in the lane marker (green circle). The direction of the optical flow in the background is similar in the surrounding area and does not change so much for several frames. On the other hand, flow vectors detected in the raindrop have various directions. For this reason, a pixel in the raindrop candidate is removed when the variance of the flow direction is small.

The closing process is applied to the binary image $SR_b(i,j)$ and the final result is obtained after removing small regions from $SR_b(i,j)$.

Figure 5(d) shows final raindrop areas obtained from raindrop candidates of Fig.5(c).

2.2 Raindrop Detection at Night

At night, only the raindrop lit up by a headlight or the surrounding light source appears on a windshield as shown in Fig.7(a). When the light source moves in an image, the intensity near the light source greatly changes. However, the intensity away from the light source does not change so much. For this reason, in an image except for the surrounding of the light source, a bright area where temporal change of the intensity is small is detected as a raindrop. The light source area R_{light} is estimated by simple binarization because it shows high intensity in an image. The surrounding area R_{near} is obtained by applying dilation processing to R_{light}. Figure 7 (b) and (c) show R_{light} and R_{near}. Based on the following condition (2), the frame differential image $FD_t(i,j)$ is created from two consecutive images $I_{t-1}(i,j)$ and $I_t(i,j)$ in which R_{near} is masked.

$$FD_t(i,j) = \begin{cases} 1 & if \;\; I_t(i,j) > T_{dark} \;\; and \\ & \quad | I_t(i,j) - I_{t-1}(i,j) | < T_{dif} \\ 0 & otherwise \end{cases} \tag{2}$$

T_{dark} is the threshold to delete a dark background from a processing region and T_{dif} is the threshold to detect a pixel where the frame differential value is small. In experiments, T_{dark} and T_{dif} are set to 30 and 20 respectively.

An integration image $SFD_t(i,j)$ is created by adding $FD_{t-m+1}(i,j)$, $FD_{t-m+2}(i,j), \cdots, F_t(i,j)$. $SFD_t(i,j)$ is binarized by the predetermined threshold T_{sfd}.

In experiments, both m and T_{sfd} are set to 3. The labeling processing is applied to the binarized $SFD_t(i,j)$. Final raindrop areas are detected after removing labeled areas that satisfy at least one of the following conditions.

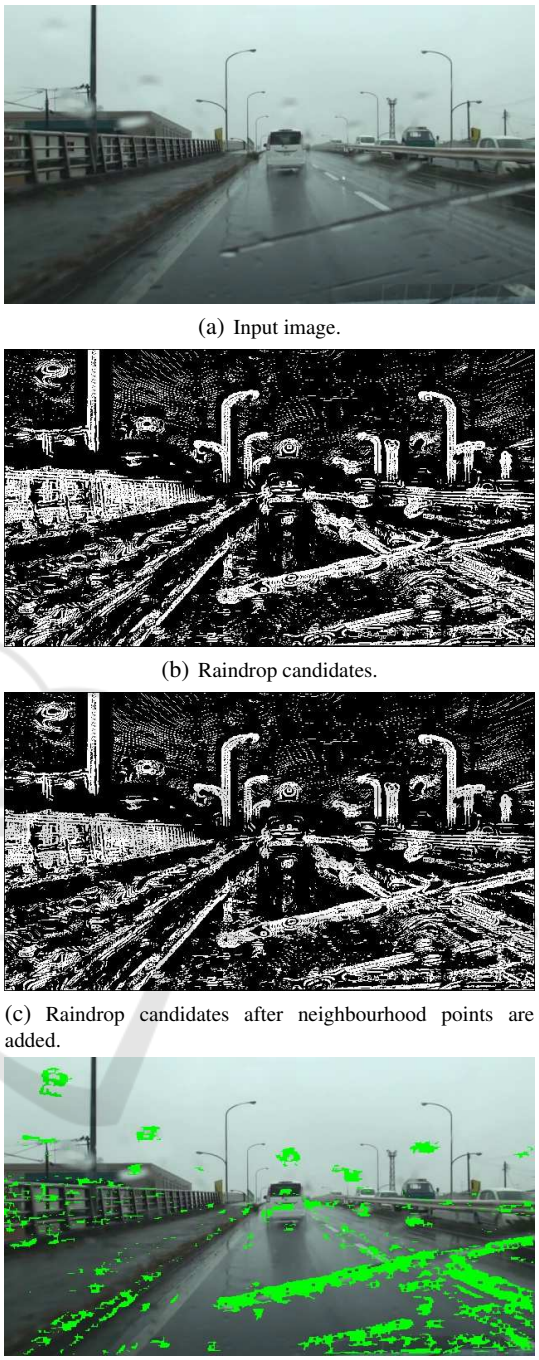

(a) Input image.

(b) Raindrop candidates.

(c) Raindrop candidates after neighbourhood points are added.

(d) Raindrop areas.

Figure 5: Raindrop detection in the daytime.

(a) Optical flow (Scene 1).

(b) Optical flow (Scene 2).

(c) Optical flow (Scene 3).

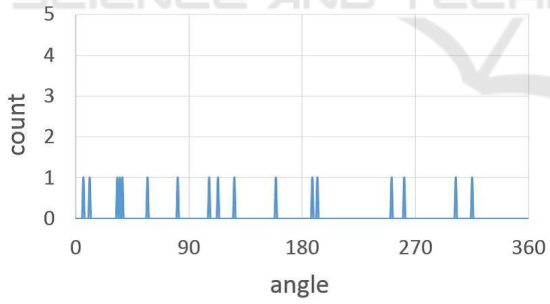

(d) Histogram created in a raindrop (blue circle).

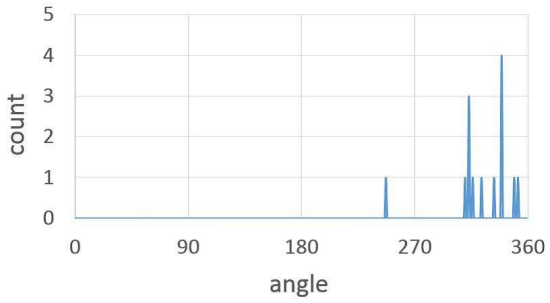

(e) Histogram created in a lane marker (green circle).

Figure 6: The direction of the optical flow.

1. R_{near} is contained in the circumscribed rectangle.
2. The size is small.

Figure 7 (d), (e), (f) and (g) show FD_{t-2}, FD_{t-1}, FD_t and $SFD_t(i,j)$. Figure 7(h) shows the final result of raindrop detection.

3 EXPERIMENTS

We conducted experiments to detect raindrops on a windshield by an in-vehicle video camera. The image size is 640×360 pixels. Eight video sequences whose length are about two minutes respectively are used for daytime experiments and six ones are used for night experiments.Various backgrounds in the main road and the community road are included in these video sequences.These video sequences also contains various rain conditions from heavy rain to light rain. In each video sequences, same parameters were used.

Figures 8-11 show examples of detection results in the daytime. Raindrops are indicated in green. Raindrops with various shapes, e.g. a band-like shape, appear on various backgrounds, such as a road surface, a building, a tree, sky and so on. Since the proposed method detects a raindrop every pixel and it uses the ratio of edge strength to detect raindrop candidates, most of raindrops with various shapes were detected regardless of a background. Some of raindrops in the sky were not detected since our method uses fixed thresholds determined by experiments. We will develop the method to decide the threshold dynamically in the next step. The current processing time in the daytime is $10fps$ on PC with Xeon 3.2GHz CPU. However, the video rate processing would be possible by the parallelization of the process and optimization of the software.

Figures 12-14 show examples of detection results at night. Raindrops are indicated in red. Most of raindrops except for the surrounding of the light source were detected. Since the brightness of the raindrop near the light source changes intensely as the light source moves in an image, it's difficult to distinguish them from reflected light on the road surface. Although the present method excludes the surrounding of the light source from a detection area, we will improve the method in future so that a raindrop near the light source can be detected. The processing time at night is more than $30fps$ on the same PC.

4 CONCLUSION

This paper proposed the method to detect raindrops

on a windshield from an in-vehicle single camera. When it rains hard, raindrops are connected on a windshield and show various shapes even if a windshield wiper is activated. The proposed method can be applied to raindrops with various shapes, e.g. a band-like shape. In the daytime, raindrops are detected by examining the difference of the blur between the surrounding area. At night, bright areas where temporal change of the intensity is small are detected as raindrops in an image except for the surrounding of the light source. Experimental results obtained from some real streets show the effectiveness of the proposed method. In the future, we aim at reducing false detection and realizing video-rate processing on the in-vehicle CPU. We are going to create the database for raindrop detection and evaluate the performance quantitatively.

REFERENCES

K. Garg and S. K. Nayar, "Vision and Rain" International Journal of Computer Vision, Vol.75, Issue 1, pp.3-27, 2007.

P. C. Barnum, S. Narashimhan and T. Kanade, "Analysis of Rain and Snow in Frequency Space" International Journal of Computer Vision, vol.86, Issue 2-3, pp.256-274, 2010.

H. Kurihata et al., "Rainy Weather Recognition from In-Vehicle Camera Images for Driver Assistance" Proceedings of IEEE Intelligent Vehicles Symposium, pp.205-210, 2005.

H. Kurihata et al., "Detection of Raindrops on a Windshield from an In-Vehicle Video Camera" International Journal of Innovative Computing, Information and Control, Vol.3, No.6(B), pp.1583-1591, 2007.

J. C. Halimeh and M. Roser, "Raindrop Detection on Car Windshields Using Geometric-Photometric Environment of Construction and Intensity-Based Correlation" Proceedings of IEEE Intelligent Vehicles Symposium, pp.610-615, 2009.

M. Sugimoto, N. Kakiuchi, N. Ozaki and R. Sugawara, "A Novel Technique for Raindrop Detection on a Car Windshield using Geometric-Photometric Model" Proceedings of ITSC, pp.740-745, 2012.

H. Liao, D. Wang, C. Yang and J. Shine, "Video-based Water Drop Detection and Removal Method for a Moving Vehicle" Information Technology Journal, Vol.12, No.4, pp.569-583, 2013.

F. Nashashibi, R. de Charette and A. Lia, "Detection of Unfocused Raindrops on a Windscreen using Low Level Image Processing" Proceedings of International Conference on Control, Automation, Robotics and Vision, pp.1410-1415, 2010.

D. Eigen, D. Krishnan and R. Fergus, "Restoring An Image Taken Through a Window Covered with Dirt or Rain" Proceedings of ICCV, pp.633-640, 2013.

S. You, R. T. Tan, R. Kawakami and K. Ikeuchi, "Adherent Raindrop Detection and Removal in Video" Proceedings of CVPR, pp.1035-1042, 2013.

APPENDIX

(a) Input image.

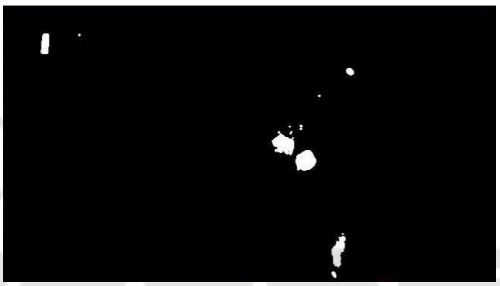

(b) Light source R_{light}.

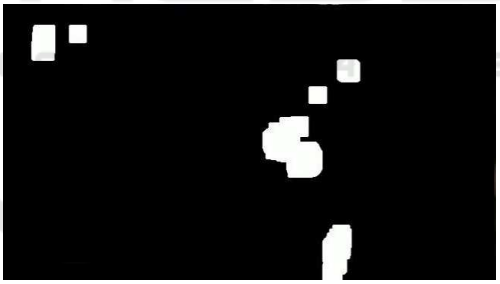

(c) R_{near}.

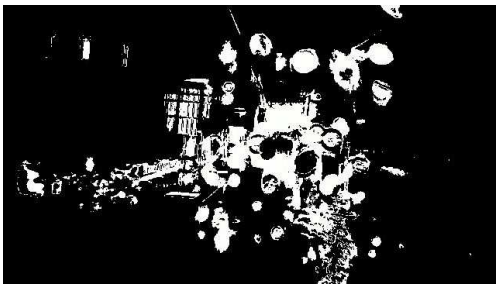

(d) $FD_{t-2}(i,j)$.

Figure 7: Raindrop detection at night.

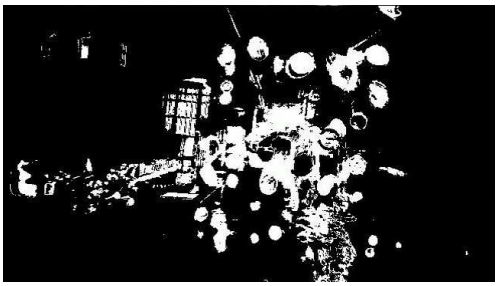

(f) $FD_{t-1}(i,j)$.

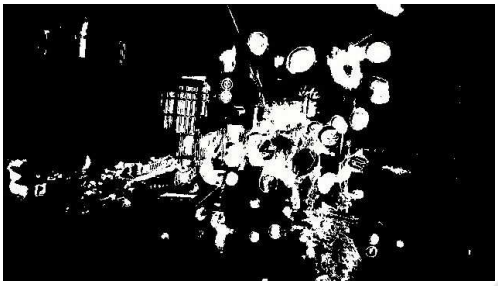

(g) $FD_t(i,j)$.

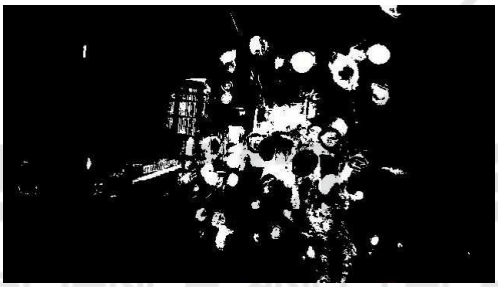

(h) $SFD_t(i,j)$.

(i) Raindrop areas.

Figure 7: Raindrop detection at night (cont.).

(a) Input image.

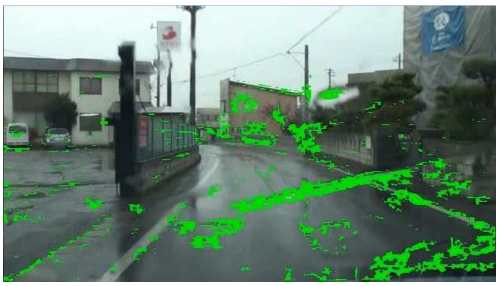

(b) Detection result.

Figure 8: Experimental results in the day time (Scene 1).

(a) Input image.

(b) Detection result.

Figure 9: Experimental results in the day time (Scene 2).

(a) Input image.

(b) Detection result.

Figure 10: Experimental results in the day time (Scene 3).

(a) Input image.

(b) Detection result.

Figure 11: Experimental results in the day time (Scene 4).

(a) Input image.

(b) Detection result.

Figure 12: Experimental results at night (Scene 5).

(a) Input image.

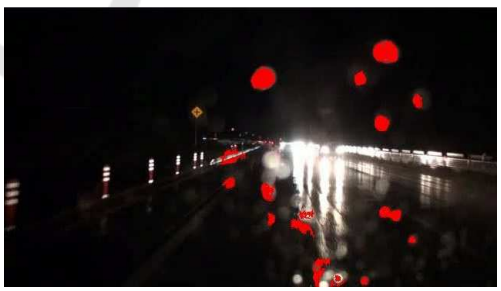

(b) Detection result.

Figure 13: Experimental results at night (Scene 6).

(a) Input image.

(b) Detection result.

Figure 14: Experimental results at night (Scene 7).